

Spin-isospin correlated configurations in complex nuclei and neutron skin effect in W^\pm production in high-energy proton-lead collisions

M. Alvioli*

*Consiglio Nazionale delle Ricerche, Istituto di Ricerca per la Protezione Idrogeologica,
via Madonna Alta 126, I-06128 Perugia, Italy*

M. Strikman†

104 Davey Lab, The Pennsylvania State University, University Park, PA 16803, USA

(Dated: August 9, 2019)

Abstract

We extend our Monte Carlo algorithm for generating global configurations in nuclei to include different spatial distributions of protons and neutrons in heavy nuclei taking into account the difference of spatial correlations between two protons, two neutrons and proton-neutron pairs. We generate configurations for ^{48}Ca and ^{208}Pb neutron-rich nuclei, which can be used in general-purpose high-energy $A(e,e'p)$, p - A and A - A event generators. As an application of lead configurations, we developed an algorithm for proton-heavy nucleus collisions at the LHC for final states with a hard interaction in the channels where cross section for p - p and p - n scattering differ. Soft interactions are taken into account in the color fluctuation extension of the Glauber algorithm, taking into account the inherently different transverse geometry of soft and hard p - N collisions. We use the new event generator to test an interesting observation of Ref. [1] that the ratio of W^\pm production rates in p - Pb collisions should significantly deviate from the inclusive value for peripheral collisions due to the presence of a neutron skin. We qualitatively confirm expectation of Ref. [1] though, for a realistic centrality trigger, we find the effect to be a factor of two smaller than the original estimate.

*massimiliano.alvioli@irpi.cnr.it

†mxs43@psu.edu

I. INTRODUCTION

It was recently pointed out that the presence of the neutron skin in heavy nuclei leads to observable effects in proton-ion collisions at LHC energies due to the difference of the cross sections of a number of hard collision processes involving quarks for pp and pn scattering [1]. The most practical case presented by the authors is the asymmetry of W^+ and W^- production cross sections. The deviations of the asymmetry from its inclusive value are larger for peripheral collisions. Thus, a study of this ratio should provide a sensitive test of the procedures used to determine centrality of the proton-nucleus and nucleus-nucleus high-energy collisions.

Increased accuracy of neutron skin measurements [2, 3] allowed comparison of measurements with state-of-the-art nuclear structure calculations [4]. Theoretical approaches and data analysis techniques should match such accuracy. This requires using descriptions of nuclei capable of including fine details of nuclear structure such as nucleon-nucleon (NN) correlations, the different extent of the neutron and proton distributions, and how NN correlations affect the distribution of the nuclear matter.

One widely used approach for the description of high-energy p-A and A-A collisions is the Monte Carlo Glauber model, whose basic ingredients are a set of Monte Carlo-generated nuclear configurations and the Glauber multiple scattering method to calculate the impact parameter dependence of individual inelastic interactions between the nucleons belonging to colliding nuclei (proton and nucleus). A number of nuclear configurations can be generated beforehand, for a given nucleus, and thus details of nuclear structure can be embedded in the configurations, and the (substantial) time needed to calculate them with the necessary accuracy can be spent only once. This approach can be used within many existing codes, for example HIJING [5], SMASH [6], Glissando [7], the Angantyr model [8], and others.

We have extended our original approach for generating nuclear configurations to include, in addition to full spin-isospin dependent NN correlations, the neutron skin effect *i.e.* the different spatial extent of the neutron and proton distributions. This can be done in principle within our method for any nucleus, even for different isotopes of the same nucleus, provided an accurate experimental determination for both the proton and neutron densities is available. In this work, we introduce fully correlated configurations for two neutron-rich nuclei, namely ^{48}Ca and ^{208}Pb . Our choice of nuclei is motivated by the use of ^{208}Pb in the

heavy ion program and the LHC, and correlation studies of e - ^{48}Ca collisions at the TJNAF.

In this paper we perform a Monte Carlo (MC) study of the W^+/W^- asymmetry, utilizing the newly generated nuclear configurations and taking into account two effects neglected in Ref. [1]: fluctuations of the number of collisions at a given impact parameter, and fluctuations of centrality determinators used in the experimental studies. Overall we find that these effects reduce the deviation of the asymmetry from its inclusive value by a factor of two, as compared to the results of Ref. [1].

The paper is organized as follows. Section 2 describes our results for nucleon configurations in ^{48}Ca and ^{208}Pb for models with uncorrelated, central-correlated and fully-correlated configurations with built-in neutron skin effect. Section 3 describes the algorithm for generating different hard interactions with protons and neutrons in combination with universal soft interactions. Definitions of centrality are presented in Section 4. Our numerical results for asymmetry are presented in Section 5, followed by conclusions in Section 6.

II. NUCLEAR CONFIGURATIONS

In this section we describe our results for ^{48}Ca and ^{208}Pb configurations calculated using an updated version of the MC code described in [9]. The original code was modified to account for neutron skin effect, the experimental and theoretical observation that the neutron density extends further from the center of the nucleus than the proton density. The code also automatically accounts for short range nucleon-nucleon (NN) correlations effects. Such effects were explicitly investigated using correlated configurations in high-energy heavy-ion collisions in Refs. [10–12].

The inclusion of the nucleon-nucleon correlations is based on the notion of a nuclear wave function ψ , which contains nucleonic degrees of freedom and which is used in our algorithm to modify iteratively the positions of randomly distributed nucleons using the Metropolis method, so that the final positions correspond to the probability density given by $|\psi|^2$. The method reproduces single particle nucleon densities [9, 13] given by the nucleus profile provided as an input, by construction, as well as the basic features of the two-nucleon density [14–23], calculated accounting for NN correlations within a number of high-precision

approaches. The model wave function is taken in the following form:

$$\psi(\mathbf{x}_1, \dots, \mathbf{x}_A) = \prod_{i < j}^A \hat{f}_{ij} \phi(\mathbf{x}_1, \dots, \mathbf{x}_A), \quad (1)$$

where ϕ is the uncorrelated wave function and \hat{f}_{ij} are nucleon-nucleon correlation operators [13]; here, \mathbf{x}_i denotes the position (\mathbf{r}_i), spin and isospin projections (σ_{zi} and τ_{zi} , respectively) of the i -th nucleon. The correlation operator contains a detailed spin-isospin structure, which is the same as the one contained in NN potentials of the Argonne family and others, which is defined as follows:

$$\hat{f}_{ij} = \sum_{n=1}^6 \hat{O}_{if}^{(n)} f^{(n)}(r_{ij}). \quad (2)$$

Here $\hat{O}_{ij}^{(n)}$ are the standard operators [24] used in the above mentioned NN potentials:

$$\hat{O}_{ij}^{(n)} = (1, \boldsymbol{\sigma}_i \cdot \boldsymbol{\sigma}_j, \mathbf{S}_{ij}) \otimes (1, \boldsymbol{\tau}_i \cdot \boldsymbol{\tau}_j). \quad (3)$$

The spatial dependence of the correlation functions $f^{(n)}$ in Eq. (2), used in this work, is shown in Fig. 1.

One-body density [9, 13, 19, 20] is defined as:

$$\rho^{(1)}(r) = \rho^{(1)}(\mathbf{r}_1)|_{r_1=r} = A \int \prod_{i=2}^A d\mathbf{r}_i^2 |\Psi(\mathbf{r}_1, \dots, \mathbf{r}_A)|^2 \quad (4)$$

and two-body density as:

$$\rho^{(2)}(\mathbf{r}_1, \mathbf{r}_2) = A(A-1) \int \prod_{i=3}^A d\mathbf{r}_i^2 |\Psi(\mathbf{r}_1, \dots, \mathbf{r}_A)|^2. \quad (5)$$

The densities in Eqs. (4) and (5) are spin-isospin summed quantities. If the summations (not shown in Eqs. (4) and (5)) over the individual isospin variables of particle “1”, in Eq. (4), and of particles “1” and “2”, in Eq. (5), are not carried out, partial quantities can be obtained. In particular, we can investigate the proton and neutron contributions to the one-body density, and the different proton-proton, proton-neutron and neutron-neutron contributions to the two-body density. In particular, we consider the radial two-body density:

$$\rho^{(2)}(r_{12}) = A \int d\mathbf{R} \rho \left(\mathbf{r}_1 = \mathbf{R} + \frac{1}{2}\mathbf{r}, \mathbf{r}_2 = \mathbf{R} - \frac{1}{2}\mathbf{r} \right). \quad (6)$$

The quantities presented in Eqs. (4) and (6) can be calculated straightforwardly using the nuclear configurations.

We produced configurations using three different approximations, namely i) the no-correlation approximation, ii) a repulsive, central correlation function, iii) a realistic set of spin- and isospin-dependent correlation functions, obtained using variational calculations of medium-heavy nuclei [15]. The approximation i) is provided as a baseline, and it can be achieved simply by imposing that the one-body density calculated from the MC configurations reproduces a Woods-Saxon parametrization of the nucleus profile. The approximation of ii) was already introduced in Ref. [9], and it can be achieved by introducing the additional constraint that the produced configurations maximize the objective function, the square of Eq. (1), where the only central correlation, $f^{(n=1)}(r_{ij}) = f^{(c)}(r_{ij}) = 1 - e^{-0.9r^2}$ [9], is retained in Eq. (2). The approximation iii) was not implemented in the original version of our MC code [9] and it was partially implemented in a previous study of initial-state anisotropies in heavy-ion collisions from the Monte Carlo Glauber (MCG) model [10]. In this paper we present results for fully correlated nuclear configurations, obtained by introducing NN correlations generated by including up to the tensor, spin-isospin-dependent operator in Eq. (2). This way we effectively take into account the three-body-induced correlations, arising from the non-commutative nature of the tensor operator which only survives in the operator chains including three particles. A nice discussion of this effect and a graphical representation of the tensor operator acting on three nucleons was presented in Ref. [17].

Inclusion of neutron skin effects in the nuclear configurations required a different parametrization for the neutron and proton densities. Each configuration is generated producing the position of A nucleons, distributed with a density $\rho(r)$ described by Woods-Saxon distributions with different parameters for protons and neutrons.

For the ^{48}Ca nucleus, we use here the parametrization of Ref. [25] for charge (proton) and neutron densities. The parametrization of Ref. [25] has the three-parameter Fermi model form:

$$\rho(r) = \frac{\rho_0 (1 + w r_{p,n}^2 / c_{p,n}^2)}{1 + e^{(r_{p,n} - c_{p,n}) / z_{p,n}}}, \quad (7)$$

where $w = -0.08$, $c_p = 3.81$ fm, $c_n = 4.12$ fm, $z_p = 0.53$ fm and $z_n = 0.51$ fm, and ρ_0 is the density at the center of the nucleus.

For the ^{208}Pb nucleus, we followed the parametrization of Ref. [3], which has the following form (a similar approach was recently adopted in Ref. [26]):

$$\rho^{(p,n)}(r) = \frac{\rho_0}{1 + e^{(r - R_0^{p,n}) / a_{p,n}}}. \quad (8)$$

The neutron radius R_0 and skin depth a_n Woods-Saxon parameters ($R_0^n = 6.7$ fm, $a_n = 0.55$ fm) were obtained in Ref. [3] using coherent pion photoproduction data while the proton ones ($R_0^p = 6.68$ fm, $a_n = 0.447$ fm) are commonly taken from high-energy elastic electron scattering measurements [27]. Results for the one-body density of ^{208}Pb are shown in Fig. 2. The figure shows a comparison of the ratio of the proton one-body density, $\rho^{(p)}(r)$, to the neutron one-body density, $\rho^{(n)}(r)$. The densities were calculated using our MC code, with uncorrelated, central-correlated and fully-correlated configurations, and compared to the experimental measurements of Ref. [3]. All of the calculated densities compare well with the measured ratio, as they should, since the inclusion of NN correlations does not affect the nucleus profile.

Figure 3 shows the radial two-body densities (*cf.* Eq. (6)) for both the considered nuclei, which we can also consider as the probability of finding a given NN pair in the nucleus at relative distance r_{12} . The different contributions from proton-proton, proton-neutron and neutron-neutron pairs in Fig. 3 are shown separately. The figure shows two-body distributions obtained with the generated configurations, highlighting the striking differences between correlated and uncorrelated configurations, including skin effect, for all the three approximations described above. In particular, the inclusion of NN correlations results in vanishing two-body densities at zero pair separation. Moreover, the fully-correlated density overshoots the central-correlated one at NN separations between 1.0 and 2.0 fm. This feature is entirely due to pn pairs, as it is evident from Figure 3(b).

Configurations including full two-body and three-body induced correlations, and including also nuclear deformations where applicable, were produced for other nuclei: ^{12}C , ^{40}Ca , ^{48}Ca , ^{63}Cu , ^{197}Au , ^{238}U , which will be presented elsewhere. All configurations will be posted on our project webpage [44]. Configurations for ^{208}Pb were also used in Ref. [28] for a different purpose, namely the study of double partonic interactions.

III. HARD TRIGGER GEOMETRY

The basic quantity calculated in the MCG approach, using the nuclear configurations described in Section II, is the probability of the projectile proton to experience ν inelastic (soft) interactions with the nucleons of the target nucleus. In particular, for the purpose of this work, we are interested in calculating the separate contributions from protons and

neutrons in the target, which we denote as $P^{soft,(p;n)}(b, \nu)$.

We can calculate the most general form of the probability of interaction with ν nucleons, with N_p protons and with N_n neutrons, as a function of both ν and of the impact parameter, and subsequently we can single out only the b dependence, as follows:

$$P^{soft,(p;n)}(b) = 2\pi b \sum_{\nu} P_{\nu}^{soft,(p;n)}(b), \quad (9)$$

or the only ν dependence, integrating over \mathbf{b} , as follows:

$$P^{soft,(p;n)}(\nu) = \int d\mathbf{b} P^{soft,(p;n)}(b, \nu), \quad (10)$$

where *soft* indicates that inelastic interactions were restricted to soft ones.

In a previous work [29], we introduced a method to further require that an event contained a hard interaction. Correspondingly, we calculated the probability $P_{ev}^{hard}(b, \nu)$ of having an event in which ν inelastic interactions occurred, one of which was a hard interaction, for the scattering of a proton on a nucleus at the impact parameter b .

Since the location of the hard interaction on the transverse plane is unknown, we can calculate the cross section differential in impact parameter by taking the convolution of the generalized parton distributions F_g of the projectile and target nucleons, and then integrate over all the possible transverse positions for each hard interaction and for each simulated p-Pb event. In each event, we select one particular nucleon as the one experiencing the hard interaction, based on the probability of hard interaction, which for each nucleon j is obtained as:

$$p_j = \frac{F_g(\mathbf{b} + \boldsymbol{\rho} - \mathbf{b}_j)}{\sum_k F_g(\mathbf{b} + \boldsymbol{\rho} - \mathbf{b}_k)}, \quad (11)$$

where the \mathbf{b} is the incoming proton's impact parameter, $\boldsymbol{\rho}$ is its transverse distance from the hard interaction point and \mathbf{b}_j is the j -th target nucleon transverse position. Figure 4 is an illustration of the transverse geometry.

Once one target nucleon is selected as the hard-interacting one, we calculate the number of soft-interacting nucleons among the remaining $A - 1$ nucleons in the target, and obtain the probability of events with a hard trigger as follows:

$$P_{ev}^{hard,(p;n)}(\nu) = \frac{1}{A} \int db d\boldsymbol{\rho} \prod_{j=1}^A d\rho_j F_g(\rho) \sum_{i=1}^A F_g(\rho_i) p(\nu; event), \quad (12)$$

where $p(\nu; event)$ is the probability that in, a specific event, ν inelastic collisions occurred, including the hard one. We keep the dependence on the particular event here, because

that is the stage at which we integrate the position of the hard interaction over the whole transverse plane, in each simulated event.

Figure 5 presents the quantities $P^{soft;hard}(b, \nu)$ calculated using the method outlined above, both in the Glauber approximation. A second method includes the effects of fluctuations of NN cross section were first introduced by [30–32], and implemented in the MCG model in [33]. The implementation is straightforward as it requires simply introducing the probability distribution over the strength of the p-N interaction [33]. Various aspects of fluctuations in p-A and A-A collisions using our configurations at LHC and RHIC energies were investigated in [29, 33, 34].

The various quantities in Fig. 5 depend only on ν , as they were integrated over the impact parameter as in Eq. (10), and both averaged over a significant number of events. The figure illustrates the effect of CF on the probability distributions as a function of the number of collisions ν . Both the distributions in Fig. 5(a) were obtained with the standard MCG model, with fixed p-N cross section, while the distributions in Fig. 5(b) were obtained including an event-by-event fluctuating p-N cross section σ_{in}^{pN} , *i.e.* with account of CF effects. It is evident that the the distributions including CF extend to much larger values of ν , as a consequence of the smearing of centrality due to the event-by-event fluctuation of the p-N cross section [33].

We calculate the probability that the projectile experiences one hard interaction in an event containing a total of ν interactions. By construction, $\nu - 1$ of them are soft interactions. We can distinguish these quantities for proton and neutrons, that is, distinguish when the hard interaction occurred with a proton or with a neutron in the target. Figure 6 shows the proton-to-neutron ratio of $P^{hard}(\nu) = \langle \int d\mathbf{b} P_{ev}^{hard}(b, \nu) \rangle$ distributions. In the figure, we show quantities calculated with: i) the Glauber approximation and un-correlated configurations, ii) Glauber and fully correlated configuration, and iii) Glauber and CF, with un-correlated configurations. We can see that CF effects are about 10% in the most peripheral events, while correlations effects are rather small and go in the opposite direction. In the following, we will investigate these features in individual centrality bins, first for the proton-to-neutron ratio, and eventually for the W^+/W^- cross sections ratio.

The probabilities defined in Eq. (10) can be integrated in the intervals of centrality

calculated as in Eq. (18), for events with a hard trigger, *i.e.*:

$$P_{ev,i}^{hard}(\nu) = \int_{b_i}^{b_{i+1}} d\mathbf{b} P_{ev}^{hard}(b, \nu), \quad (13)$$

and then calculate the average number of collisions, in each centrality bin, as follows:

$$\langle \nu^{p,n} \rangle_i = \frac{\sum_{\nu} \nu P_{ev,i}^{hard(p)}(\nu)}{\sum_{\nu} P_{ev,i}^{hard(n)}(\nu)}. \quad (14)$$

Note that in Eq. (14) we have distinguished the cases when the hard interaction occurred with a proton or with a neutron, so that we can calculate the ratio

$$\langle \nu^p \rangle_i / \langle \nu^n \rangle_i. \quad (15)$$

To estimate the ratio of the W^+ to W^- production we need to take into account that the corresponding cross sections depend on the quark content of the nucleons. Namely, W^+ production on neutrons occurs with a probability a , relative to W^+ production on protons, and vice-versa for W^- production. We introduced this dependence in our MCG code calculating new probabilities which incorporate different weights for W production on protons and neutrons, *i.e.* with different values of a in the definition of the relative probability.

IV. DEFINITION OF CENTRALITY

As a first approximation, we define centrality bins with respect to impact parameter b as follows. Based on the definition of the total inelastic cross section:

$$\sigma_{in}^A = \int d\mathbf{b} \sum_{n=1}^A \sigma_n(b), \quad (16)$$

the k -th term in the above equation being:

$$\sigma_n(b) = 2\pi b \binom{n}{A} \left(\sigma_{in}^{pN} T(b) \right)^n \left(1 - \sigma_{in}^{pN} T(b) \right)^{A-n}, \quad (17)$$

with $\sigma_{in}^{pN} = \sigma_{tot}^{pN} - \frac{\sigma_{tot}^{pN^2}}{4\pi B_0^2}$, we define bins in b , $[b_i, b_{i+1}]$, such as:

$$f_i = \frac{1}{\sigma_{in}^A} \int_{b_i}^{b_{i+1}} d\mathbf{b} \sigma_n(b) \quad (18)$$

where $f_i = \{0, 0.1, 0.2, 0.3, 0.4, 0.5, 0.6, 0.7, 0.8, 0.9, 1\}$ as required to compare with the results of Ref. [1].

The definition of centrality was refined following the method used in experimental analyses, using the ATLAS experiment studies of centrality as follows. The correlation between hadron production at central rapidities and at $-4.9 < \eta < -3.2$ in the nucleus outgoing direction in p-A collisions at $\sqrt{s} = 5$ TeV can be interpreted in the framework of CF [35] phenomena. Due to the approximate Feynman scaling near the nuclear fragmentation region, energy conservation effects are not expected to affect the total transverse energy, ΣE_T , or to be strongly correlated with the activity in the rapidity-separated central and forward rapidities regions. This expectation is validated by a measurement of ΣE_T as a function of hard scattering kinematics in p-p collisions [36]. Distributions of ΣE_T were constructed as a function of the number of participating nucleons, $\nu + 1$. Simple Glauber estimates of ν resulted in ΣE_T distributions narrower than those observed in the data. Using the CF approach, instead, leads to a broader ν distribution due to the $\sigma_{in}^{pN} > \langle \sigma_{in}^{pN} \rangle$ tail of the distribution for p-N inelastic cross section $P_p(\sigma_{in}^{pN})$ [31], and produces overly broad ΣE_T distributions. Based on these observations, parametrization of ΣE_T was built and used to calculate the relative contributions from collisions with different ν values to the p-A centrality classes (bins in ΣE_T) used by the ATLAS collaboration. Application of the ΣE_T parametrization to our case leads to the centrality classes shown in Fig. 7. The figure shows that a broad range of values for ν contribute to each centrality class, as expected from the CF approach with a fluctuating p-N cross section.

V. RESULTS

The ratio defined in Eq. (15) is shown in Fig. 8. The figure shows results for centrality classes defined by both the total inelastic cross section method and using the ΣE_T parametrization. Using the total inelastic cross section method, we find a result which is essentially consistent with the analysis of Ref. [1], in each centrality class. With this definition of centrality, the Glauber and CF results practically coincide.

At the same time using the experimental procedure for determining centrality classes we find a significant reduction of sensitivity to neutron skin effect. Account of CF effects leads to a further reduction of the sensitivity. Qualitatively the reason is that the number of

wounded nucleons at a given impact parameter fluctuates quite significantly already in the Glauber model and even more so in the CF model.

We checked the effect of NN correlations on the quantity defined by Eq. (15). We have previously done so for the proton-to-neutron ratio of inclusive $P^{hard,(p;n)}(\nu)$ probabilities, which are shown in Fig. 6. Results for the same quantity, but integrated within different centrality bins, are shown in Fig. 9. In this case we actually compared only the ratios obtained with the Glauber approach (no CF effects) and with centrality determined by the $T(b)$ method, Eqs. (17) and (18). We repeated the calculation with un-correlated and with fully-correlated configurations. The comparison in Fig. 9 reveals little effect from the inclusion of NN correlations.

The final result of our work is illustrated in Fig. 10. Experimentally the asymmetry of W^+ and W^- production, described as follows:

$$A = (d\sigma^+ - d\sigma^-)/(d\sigma^+ + d\sigma^-), \quad (19)$$

was measured at the LHC in pp scattering (for review and references see [37] with a maximal value of $A \approx 0.26$.

We show results for pretty large values of $a = d_{pn}\sigma^+/d_{pn}\sigma^- \approx d_{pp}\sigma^-/d_{pp}\sigma^+$, namely $a = 0.2$ and $a = 0.4$, corresponding to production of W in the backward kinematics where a valence quark of a nucleon annihilates with a sea antiquark of the projectile proton. In this kinematics $d_{pn}\sigma^+ = d_{pp}\sigma^-$ and $d_{pn}\sigma^- = d_{pp}\sigma^+$. We find a reduction of the ratio of W^+ to W^- production cross sections, when centrality is accounted for in an accurate way as well as color fluctuations. Typically, the deviation of the asymmetry from the inclusive value $(Z + aN)/(aZ + N)$ is reduced by a factor of two.

Eventually, we explicitly investigated the effect of using completely un-correlated or fully-correlated nuclear configurations; results are shown in Fig. 11. In both cases the inclusion of correlations provides little to no difference. The effect is smaller or equal than that on the effective proton-to-neutron ratio, both in the un-binned ratio, in Fig. 6, and in the ratio classified in centrality bins, in Fig. 9.

VI. CONCLUSIONS

We investigated the possibility of assessing centrality in pA collisions by exploiting the existence of neutron skin in the lead nucleus. The idea was originally suggested in Ref. [1], by calculating the dependence on centrality, and thus on neutron skin, of W^\pm production in pA collisions. We have investigated the same idea by including state-of-the-art accuracy calculation on many respects, introducing: (i) fully NN correlated nuclear configurations with built-in neutron skin; (ii) event-by-event fluctuation of the pN cross section (color fluctuations); (iii) accurate classification of centrality, following the experimental method for the definition of centrality bins, instead of the purely theoretical definition based on nuclear thickness, $T(b)$; (iv) a detailed trigger mechanism for the hard-interacting particles.

In order to ensure a realistic treatment of the nucleus wave function in modeling high-energy collisions involving nuclei, we extended our existing event generator to produce configurations including effects of NN correlations in different spin-isospin states and the neutron skin effect. The fully-correlated ^{48}Ca and ^{208}Pb configurations show the signatures of short-range correlations [17, 19], which are mostly found in two-body densities and can be summarized as: a) vanishing probability of finding two nucleons at zero spatial separation, regardless of the nucleons' kind; b) the pair probability has a maximum for $1.0 \text{ fm} \lesssim r_{12} \lesssim 2.0 \text{ fm}$; b) the pn probability has a more pronounced peak than pp and nn pairs, which is also found for the total two body density (*cf.* Fig. 3). The newly generated configurations for ^{48}Ca and ^{208}Pb also include neutron skin effect, and are available for download as plain text tables, along with configurations for other nuclei.

Configurations are readily usable by any code which is based on Monte Carlo Glauber models [5, 7] and for any kind of derived model for applications possibly different from the one presented in this work, such as any p-A and A-A numerical model which takes nucleon positions as an input [6, 34, 38, 39], also in combination with models for p-p studies which can be implemented within processes involving nuclei [8, 40].

In this work, an application of the generated configurations, in particular of the possibility of describing nuclei using configurations with built-in NN correlations and neutron skin, is provided. With the aim of assessing the possibility of exploiting the existence of a neutron skin in the nucleus of lead [2, 3], we considered the W^\pm production ratio in pA collisions. We investigated separately the effects of the points (i)-(iii) above. Point (iv), consisting in

the use of an advanced hard interaction trigger for the elementary pN collisions, was used throughout the paper, instead.

We calculated results, using different approximations, for two quantities; the most basic effective proton-to-neutron ratio (Figs. 8, 9), and the actual quantity we are interested in, the W^+/W^- cross sections ratio (Figs. 10, 11). In both quantities, we investigated separately the effects of the approximations (i)-(iii) listed above. Our findings can be summarized as follows:

- figure 8 shows a comparison of the results for the proton-to-neutron ratio, as a function of centrality classes, obtained according to: (a) the most basic approximation, in which centrality is accounted for using cuts in the integral of the nuclear thickness function $T(b)$, Eq. (18), as in Ref. [1] (Glauber, $T(b)$); (b) the next approximation, in which centrality is accounted for using the experimental parametrization for hadronic activity [35], as in Refs. [41, 42] (Glauber, ΣE_T); (c) the most advanced model, in which centrality is obtained as in (b) and color fluctuations effects are taken into account by means of event-by-event fluctuation of the pN inelastic cross section [29, 33, 41, 42] (GL + CF, ΣE_T). Results show that deviations of the ratio from its nominal value are strongly reduced in the most accurate estimate, with respect to the no CF, simple centrality classification method, and both the ΣE_T classification method and CF effects are relevant to the result;
- figure 9 shows explicitly the effects of NN correlations, in the case of centrality classification using $T(b)$, Eq. (18). The results were obtained using different nuclear configurations, either generated with and without inclusion of NN correlations, but including neutron skin in both cases. We can see that NN correlations plays little role in the effective proton-to-neutron ratio determination;
- figure 10 shows our estimate of the σ^+/σ^- ratio, as a function of centrality classes. Results are presented for two values of the parameter a , the relative weight of production of W^+ from neutrons with respect to protons, or of W^- from protons with respect to neutrons (see Section V). For both values of the parameters, we find that the deviation of the ratio calculated with the simplest approximation (Glauber, $T(b)$) is reduced by about 50% if the most advanced approximation is used (GL + CF, ΣE_T);

- figure 11 shows explicitly the effect of including or not including NN correlations in the calculations on the σ^+/σ^- ratio, as a function of centrality. The effect is shown to be negligible for both the simplest approximation (Glauber, $T(b)$) and for the most accurate one (GL +CF, ΣE_T).

In conclusion, we confirmed the observation of Ref. [1] that the ratio of the rates of production of W^+ and W^- in p-Pb collisions should depend on centrality of the collision due to the presence of the neutron skin, though the inclusion of color fluctuation effects caused a reduction of the previously predicted strength of the dependence on centrality. We also found that the expected centrality dependence of the ratio is sensitive to the model used to determine centrality, making this process a good testing ground for checking the centrality models especially for peripheral contributions.

Eventually, we argue that it would be possible to extend the calculation of the W^+/W^- ratio in peripheral Pb-Pb collisions, as in Ref. [43], by including the effects of fluctuations, for an improved accuracy in modeling peripheral heavy ion collisions at collider energies.

Acknowledgments

The research of M.S. was supported by the U.S. Department of Energy, Office of Science, Office of Nuclear Physics, under Award No. DE-FG02-93ER40771. M.A. acknowledges a CINECA award under ISCRA initiative for making high-performance computing resources available.

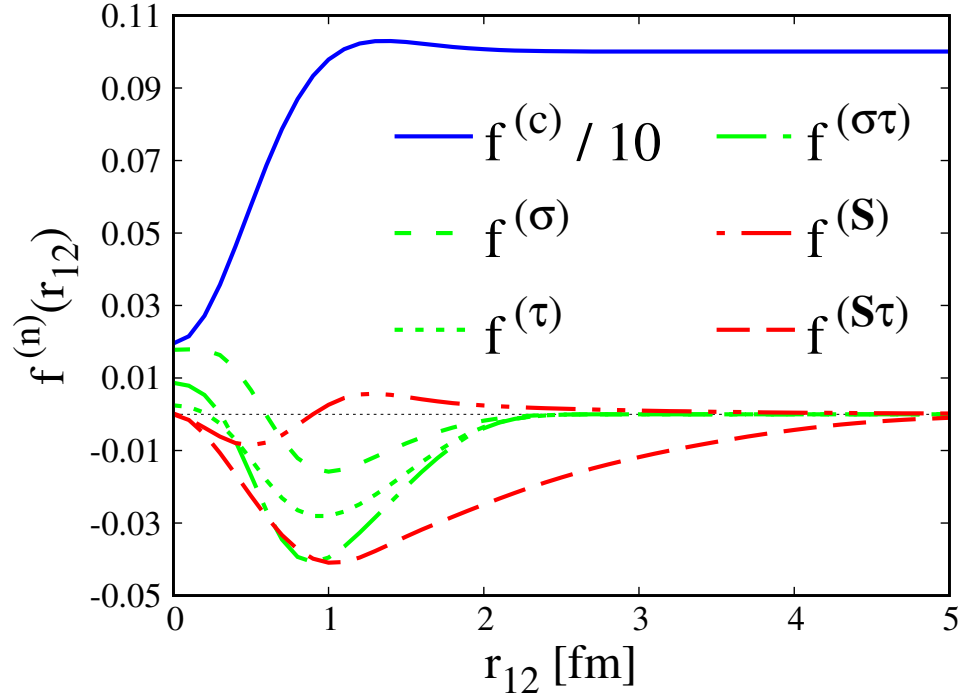


FIG. 1: The spatial dependence of the correlation functions $f^{(n)}(r_{ij} = r_{12})$ appearing in Eq. (2). Each of the functions shown in the figure couples with the corresponding spin-isospin-dependent operator in Eq. (2). From Ref. [13].

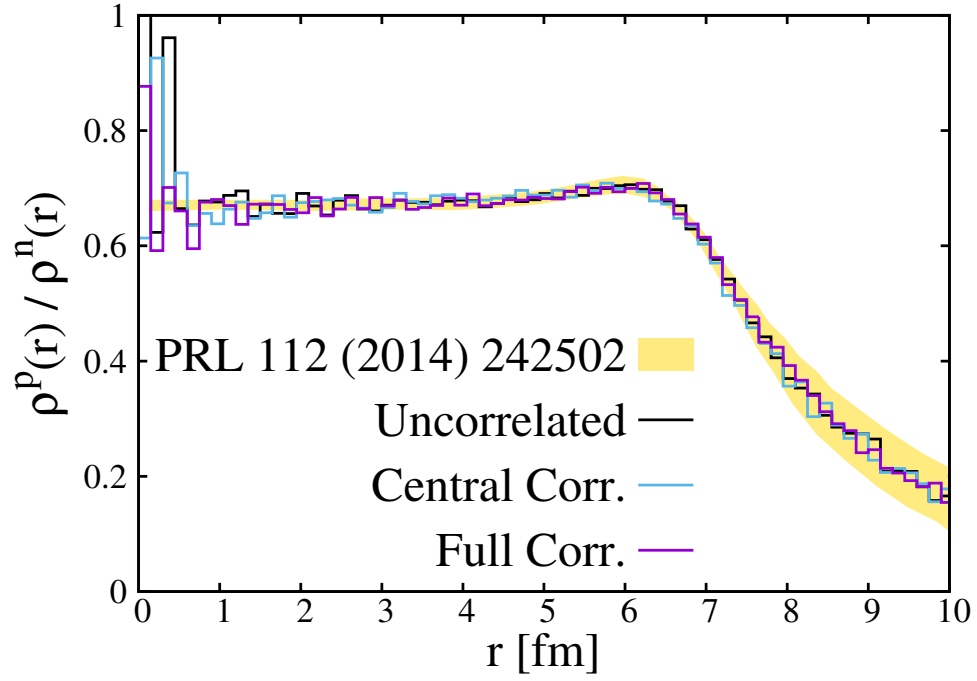


FIG. 2: The proton-to-neutron ratio of one-body densities as defined in Eq. (4), compared with the experimental data from Ref. [3]

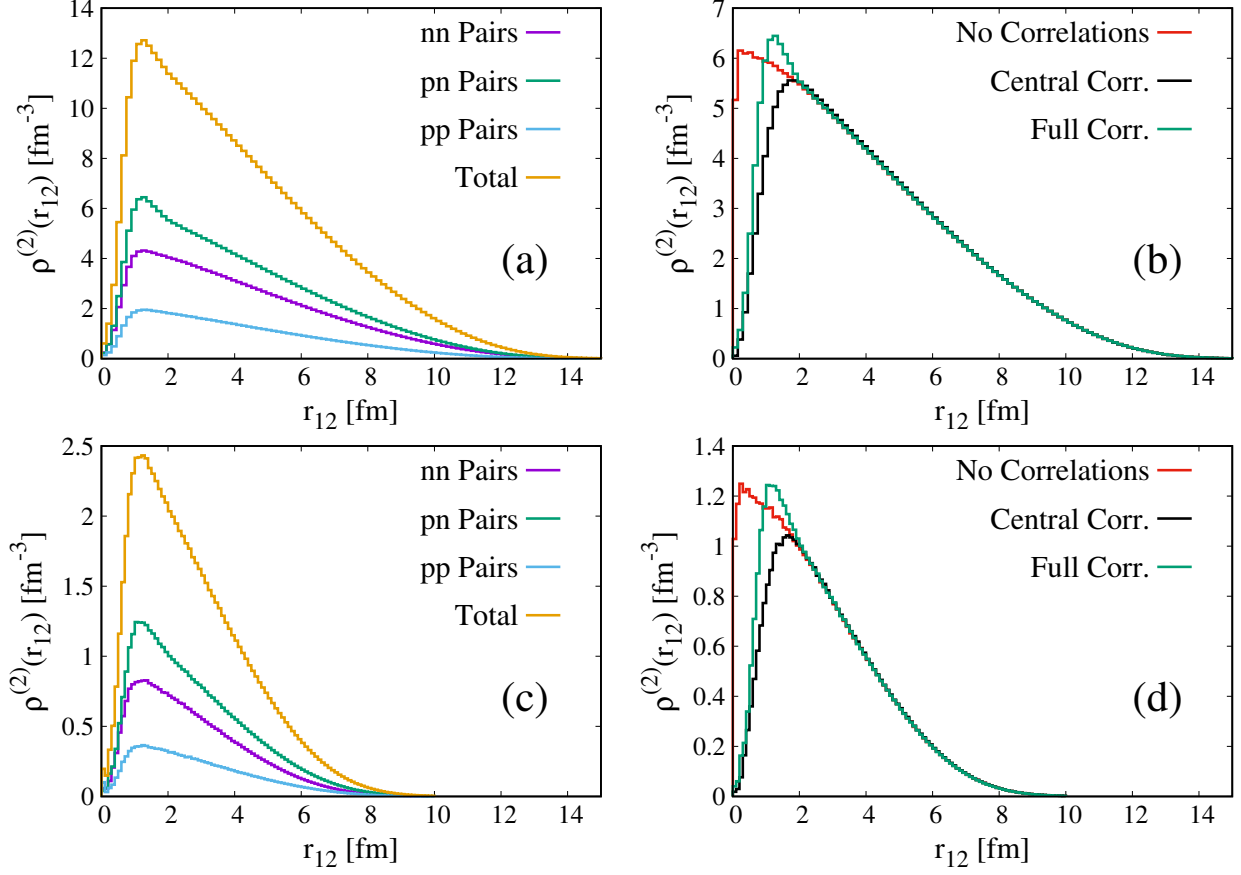


FIG. 3: The two-body density of ^{208}Pb , in (a) and (b), and of ^{48}Ca , in (c) and (d) as defined in Eq. (6), obtained with our configurations. (a) and (c): curves corresponding to different nucleon pairs, proton-proton (pp), proton-neutron (pn) and neutron-neutron (nn), whose sum is the total two-nucleon density (Total). (b) and (d): the effect of correlations in the case of proton-neutron pairs. All the curves are normalized according to the corresponding number of pairs in the nucleus.

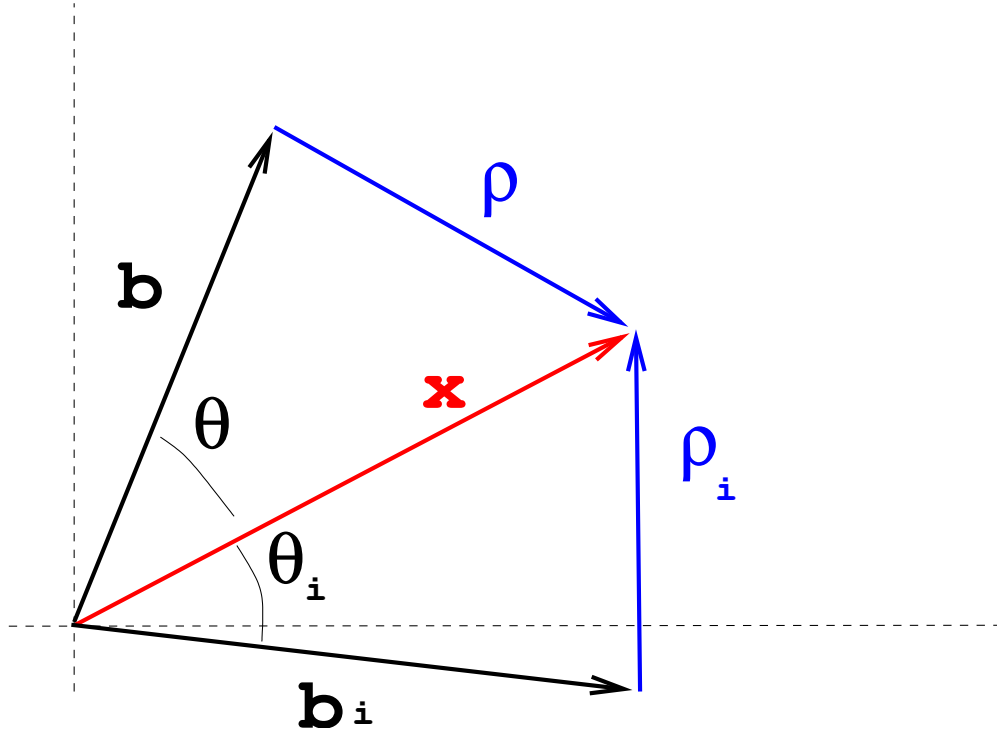


FIG. 4: Sketch of the transverse geometry of a hard collision, occurring at the location pointed by the vector x . The vector \mathbf{b} points to the position of the incoming proton, and \mathbf{b}_i to the i -th target nucleon. From Ref. [29].

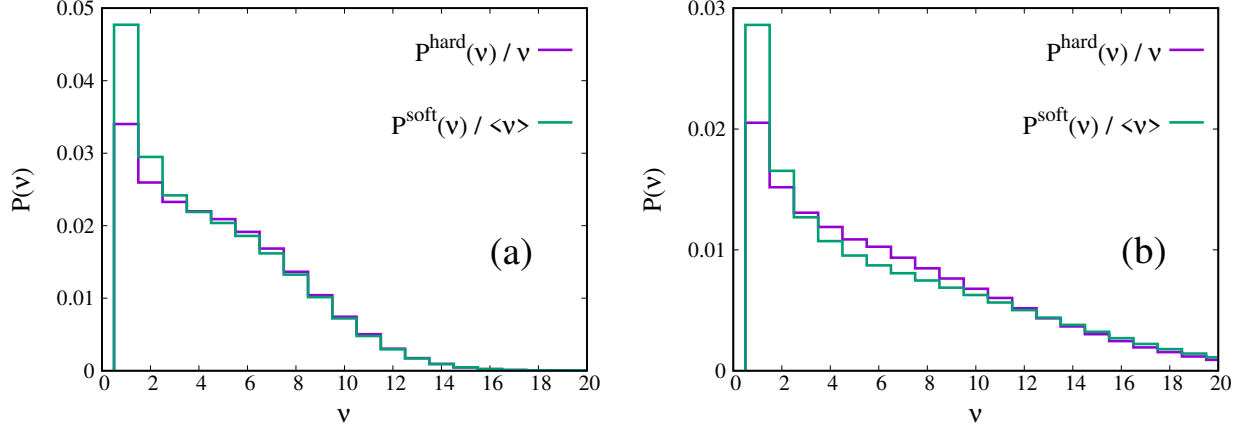


FIG. 5: Analysis of the soft and hard probabilities of interaction as a function of the number of collisions ν . In both panels, we compare the quantity $P^{\text{hard}}(\nu)/\nu$ with $P^{\text{soft}}(\nu)/\langle\nu\rangle$. All calculations are independent of neutron skin effects, and the protons and neutrons were not distinguished, for the sake of illustration of the color fluctuations effect, which is absent in (a), and included in (b).

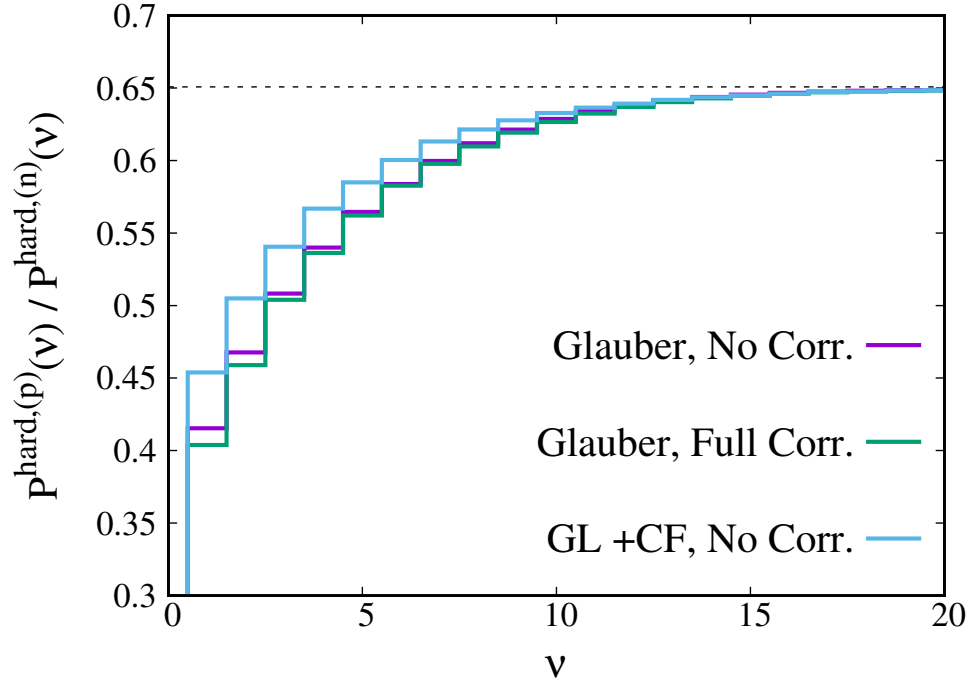


FIG. 6: The proton-to-neutron ratio of the probability $P^{\text{hard}}(\nu)$, calculated selecting only proton or neutrons in the target; we show separately the effects of NN correlations and of color fluctuations, for illustration purposes. The horizontal dashed line corresponds to Z/N .

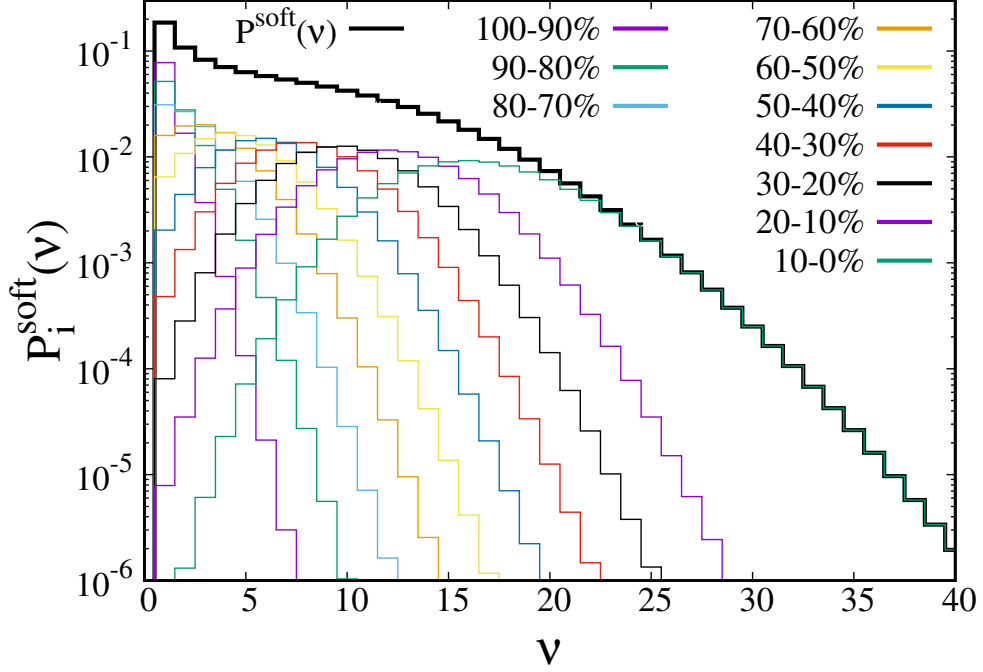


FIG. 7: The probability of interaction $P^{soft}(\nu)$, calculated within the color fluctuations approximation, and the different contributions to each centrality bin, according to the most accurate definition of centrality, based on ΣE_T . The thick black line shows the total probability; we did not distinguish between protons or neutrons, here.

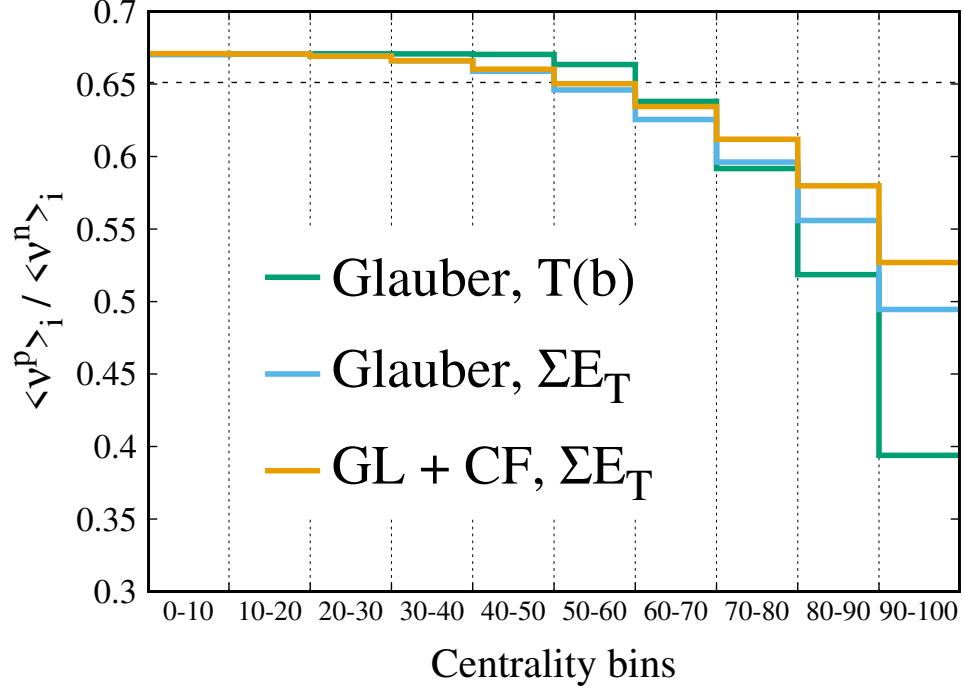


FIG. 8: The effective proton-to-neutron ratio. Green curve: the most basic approximation (comparable with the results of Ref. [1]), where we used the definition of centrality based on the thickness function integral, (T(b)) and Glauber model. Blue curve: Glauber model with definition of centrality based on experimental model (ΣE_T). Gold curve: the most refined approximation, where we used the experimental definition of centrality and included color fluctuations (CF) effects. The horizontal dashed line corresponds to Z/N .

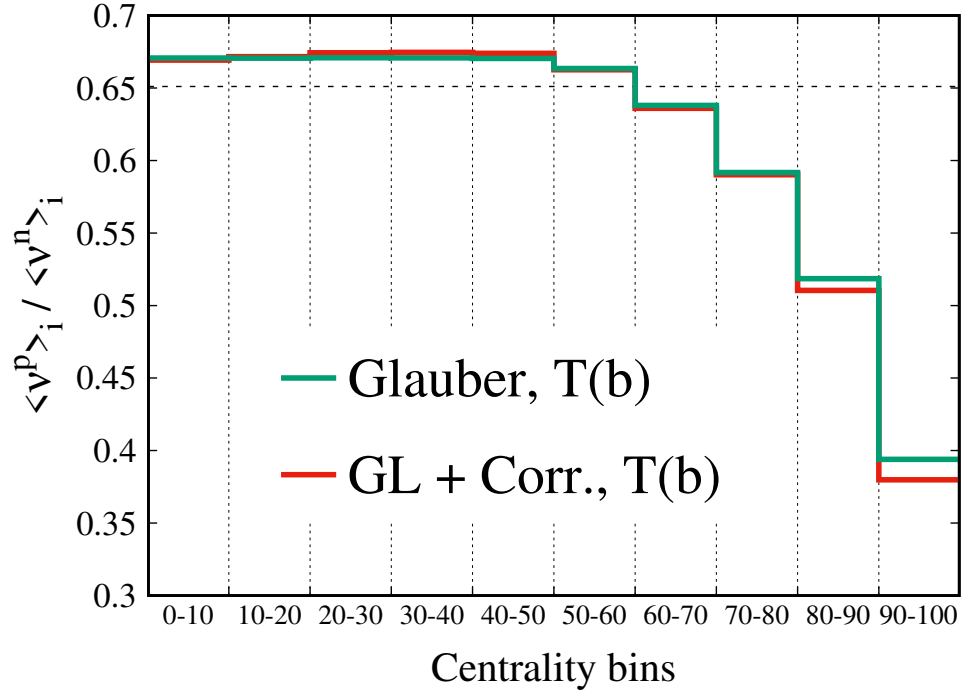


FIG. 9: Inclusion of correlated configurations on the effective proton-to-neutron ratio, in the simplest Glauber approximation and centrality defined using $T(b)$ (also shown in Fig. 8). The effect of NN correlations is very weak. The horizontal dashed line corresponds to Z/N .

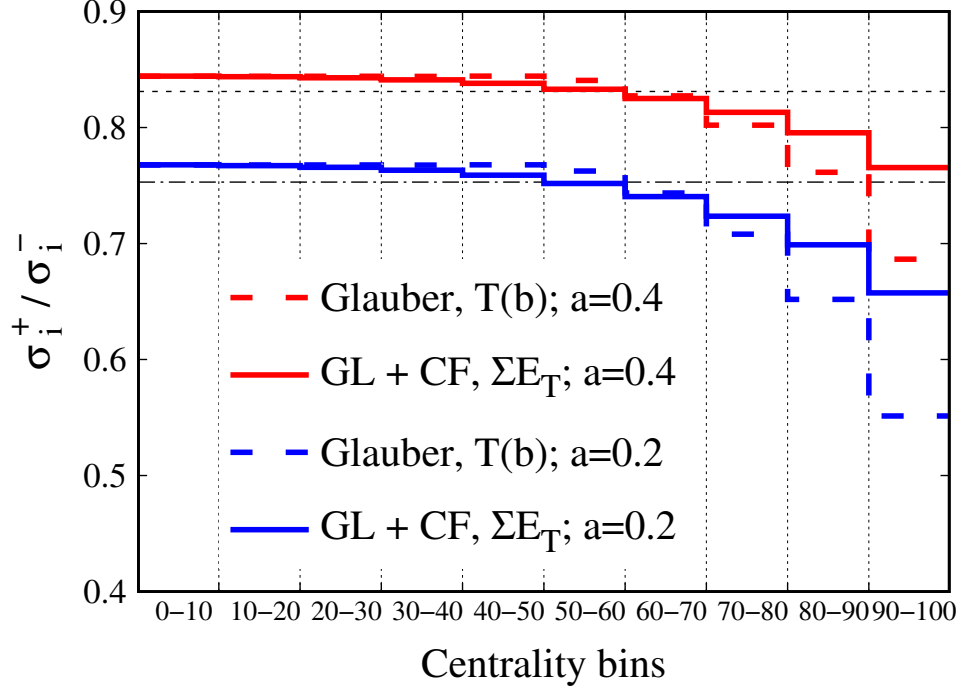


FIG. 10: The ratio of the W^+ production cross section to the W^- one, calculated assuming $\sigma_i^+ \propto P_i^{hard(p)} + a P_i^{hard(n)}$, and $\sigma_i^- \propto a P_i^{hard(p)} + P_i^{hard(n)}$, to account for the different d and u quark content of protons and neutrons. The dashed and dot-dashed horizontal lines correspond to the quantity $(Z + aN)/(aZ + N)$, for $a = 0.4$ and $a = 0.2$, respectively.

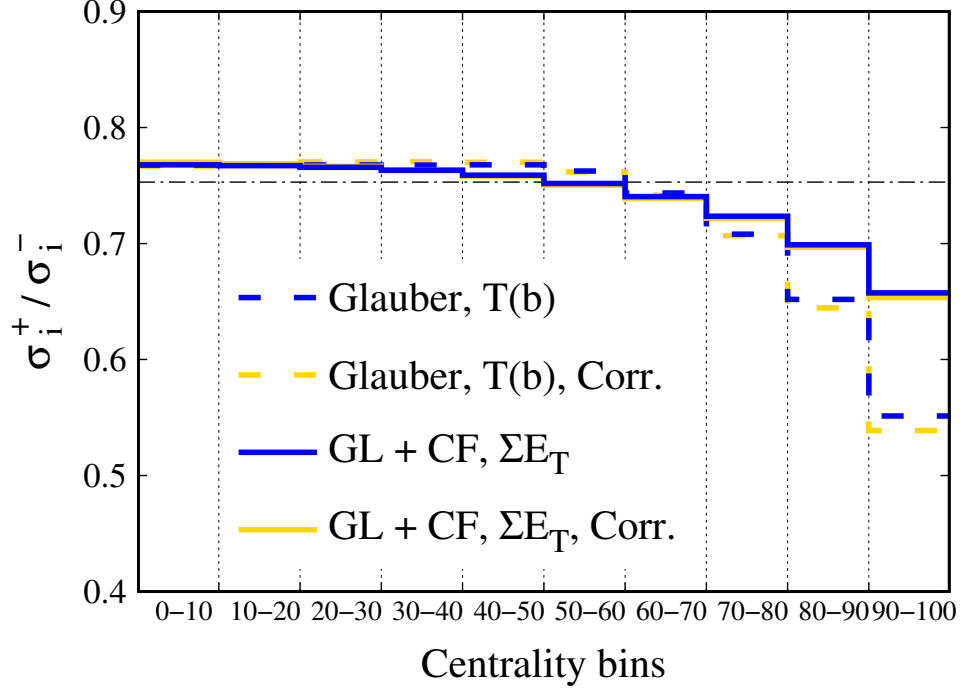


FIG. 11: Inclusion of nucleon-nucleon correlations on the ratio of the W^+ production cross section to the W^- one, defined as in Fig. 10. We compare the results in the case $a = 0.2$ (blue curves, also shown in Fig. 10), with the corresponding calculations including correlations (yellow curves). Dashed lines correspond to the most basic approximation, where no CF nor accurate centrality definitions were accounted for; both effects are present in the calculation of solid lines. In both cases the inclusion of correlations provides little to no difference. The dashed and dot-dashed horizontal line correspond to the quantity $(Z + aN)/(aZ + N)$.

-
- [1] H. Paukkunen, Phys. Lett. **B745**, 73 (2015).
- [2] C. J. Horowitz, K. S. Kumar, and K. S. Michaels, The European Physical Journal A **50**, 48 (2014), ISSN 1434-6001.
- [3] C. M. Tarbert et al. (Crystal Ball at MAMI and A2 Collaboration), Phys. Rev. Lett. **112**, 242502 (2014).
- [4] G. Hagen, A. Ekström, C. Forssén, G. Jansen, R. W. Nazarewicz, T. Papenbrock, K. Wendt, A., S. Bacca, et al., Nature Physics **12**, 186 (2016), ISSN 1745-2481.
- [5] W.-T. Deng, X.-N. Wang, and R. Xu, Phys. Rev. **C83**, 014915 (2011), 1008.1841.
- [6] J. Weil et al., Phys. Rev. **C94**, 054905 (2016), 1606.06642.
- [7] P. Božek, W. Broniowski, M. Rybczyński, and G. Stefanek (2019), 1901.04484.
- [8] C. Bierlich, G. Gustafson, L. Lönnblad, and H. Shah, JHEP **10**, 134 (2018), [JHEP18,134(2020)], 1806.10820.
- [9] M. Alvioli, H. Drescher, and M. Strikman, Physics Letters B **680**, 225 (2009), ISSN 0370-2693.
- [10] M. Alvioli, H. Holopainen, K. J. Eskola, and M. Strikman, Phys. Rev. C **85**, 034902 (2012).
- [11] J.-P. Blaizot, W. Broniowski, and J.-Y. Ollitrault, Phys. Rev. C **90**, 034906 (2014).
- [12] M. Alvioli and M. Strikman, Phys. Rev. C **83**, 044905 (2011).
- [13] M. Alvioli, C. C. d. Atti, and H. Morita, Phys. Rev. C **72**, 054310 (2005).
- [14] J. L. Forest, V. R. Pandharipande, S. C. Pieper, R. B. Wiringa, R. Schiavilla, and A. Arriaga, Phys. Rev. C **54**, 646 (1996).
- [15] M. Alvioli, C. Ciofi degli Atti, and H. Morita, Phys. Rev. Lett. **100**, 162503 (2008).
- [16] R. Schiavilla, R. B. Wiringa, S. C. Pieper, and J. Carlson, Phys. Rev. Lett. **98**, 132501 (2007).
- [17] H. Feldmeier, W. Horiuchi, T. Neff, and Y. Suzuki, Phys. Rev. C **84**, 054003 (2011).
- [18] M. Alvioli, C. Ciofi degli Atti, L. P. Kaptari, C. B. Mezzetti, H. Morita, and S. Scopetta, Phys. Rev. **C85**, 021001 (2012).
- [19] M. Alvioli, C. Ciofi degli Atti, L. P. Kaptari, C. B. Mezzetti, and H. Morita, International Journal of Modern Physics E **22**, 1330021 (2013).
- [20] M. Alvioli, C. Ciofi degli Atti, and H. Morita, Phys. Rev. C **94**, 044309 (2016).
- [21] D. Lonardoni, A. Lovato, S. C. Pieper, and R. B. Wiringa, Phys. Rev. **C96**, 024326 (2017).
- [22] D. Lonardoni, S. Gandolfi, X. B. Wang, and J. Carlson, Phys. Rev. **C98**, 014322 (2018).

- [23] R. Cruz-Torres, A. Schmidt, G. Miller, L. Weinstein, N. Barnea, R. Weiss, E. Piasetzky, and O. Hen, *Physics Letters B* **785**, 304 (2018), ISSN 0370-2693.
- [24] V. R. Pandharipande and R. B. Wiringa, *Rev. Mod. Phys.* **51**, 821 (1979).
- [25] G. D. Alkhalaf, S. L. Belostotsky, and A. A. Vorobev, *Phys. Rept.* **42**, 89 (1978).
- [26] C. Loizides, J. Kamin, and D. d’Enterria, *Phys. Rev.* **C97**, 054910 (2018), [erratum: *Phys. Rev.* **C99**, no.1, 019901 (2019)], 1710.07098.
- [27] M. Warda, X. Viñas, X. Roca-Maza, and M. Centelles, *Phys. Rev. C* **81**, 054309 (2010).
- [28] M. Alvioli, M. Azarkin, B. Blok, and M. Strikman, *Eur. Phys. J.* **C79**, 482 (2019), 1901.11266.
- [29] M. Alvioli, L. Frankfurt, V. Guzey, and M. Strikman, *Phys. Rev. C* **90**, 034914 (2014).
- [30] G. Baym, L. Frankfurt, and M. Strikman, *Nuclear Physics A* **566**, 149 (1994), ISSN 0375-9474.
- [31] G. Baym, B. Blattel, L. L. Frankfurt, H. Heiselberg, and M. Strikman, *Phys. Rev.* **C52**, 1604 (1995).
- [32] B. Blaettel, G. Baym, L. L. Frankfurt, H. Heiselberg, and M. Strikman, *Phys. Rev.* **D47**, 2761 (1993).
- [33] M. Alvioli and M. Strikman, *Physics Letters B* **722**, 347 (2013), ISSN 0370-2693.
- [34] M. Rybczyński, G. Stefanek, W. Broniowski, and P. Bożek, *Computer Physics Communications* **185**, 1759 (2014), ISSN 0010-4655.
- [35] G. Aad et al. (ATLAS), *Eur. Phys. J.* **C76**, 199 (2016).
- [36] G. Aad et al. (ATLAS), *Phys. Lett.* **B756**, 10 (2016).
- [37] W. Barter (ATLAS, LHCb, CMS) (2016), pp. 217–224, 1605.02487.
- [38] J. S. Moreland, J. E. Bernhard, and S. A. Bass, *Phys. Rev.* **C92**, 011901 (2015).
- [39] S. McDonald, C. Shen, F. Fillion-Gourdeau, S. Jeon, and C. Gale, *Phys. Rev.* **C95**, 064913 (2017).
- [40] K. Welsh, J. Singer, and U. W. Heinz, *Phys. Rev.* **C94**, 024919 (2016).
- [41] M. Alvioli, B. A. Cole, L. Frankfurt, D. V. Perepelitsa, and M. Strikman, *Phys. Rev. C* **93**, 011902 (2016).
- [42] M. Alvioli, L. Frankfurt, D. Perepelitsa, and M. Strikman, *Phys. Rev.* **D98**, 071502 (2018).
- [43] I. Helenius, H. Paukkunen, and K. J. Eskola, *Eur. Phys. J.* **C77**, 148 (2017).
- [44] URL: <http://sites.psu.edu/color/>